43rd AIAA Aerospace Sciences Meeting, Jan 10–13, Reno, Nevada

Direct numerical simulation of the thermal effects of plasmas on turbulent flows

Shankar Ghosh* and Krishnan Mahesh†

University of Minnesota, Minneapolis, MN, 55455, USA

The thermal effects of plasmas on isotropic turbulence are studied using direct numerical simulations. The temperature ratio of the plasma region to the background region is moderate. Two idealizations of the plasma are considered – spherical and conical. The conical idealization is found preferable in that it approximates the tear–drop shape of the plasma region that is observed experimentally, and produces baroclinic vorticity. The variation of the magnitude of the vorticity with temperature ratio and size of plasma region is examined. A blast wave followed by a region of expansion propagates normal to the axis of the plasma region. The turbulence is observed to be suppressed in the core of the plasma, presumably due to bulk expansion.

I. Introduction

Plasmas are being explored for a variety of applications such as flow control, enhanced combustion, drag reduction, and vehicle steering (e.g. Knight et al 2003, Adelgren et al 2003, Schneider et al 2003). A variety of approaches may be used to generate plasmas, one of which is laser induced breakdown of a gas (Maker et al. 1963, Damon & Tomlinson 1963, Meyerand & Haught 1963). The breakdown is described by four successive stages (Raizer 1997): the initial release of electrons due to multi-photon collision with gas molecules, ionization of the gas in the focal region by cascade release of electrons and formation of the plasma, formation of a blast wave due to absorption of laser energy by the plasma, propagation of the blast wave into the surrounding gas and formation of a residual vortex ring. Prominent features of this phenomenon are that the plasma region is tear–drop shaped, the blast wave evolves from a non–spherical to a spherical shape and a toroidal vortex ring is generated.

Recent experimental work on pulsed laser induced breakdown in quiescent air or nitrogen, include Jiang et al. (1998), Lewis et al. (1999), Dors et al. (2000), Adelgren et al. (2001) and Yan et al. (2003). Jiang et al. (1998) used a laser beam of 1.38 J focused on a 3 mm diameter spherical region to cause breakdown in air. The laser was pulsed for 18 nanoseconds duration. Dors et al. (2000) used a 50 mJ laser beam pulsed for a duration of 5 nanoseconds in quiescent nitrogen over a volume of 0.21 mm^3. Adelgren et al. (2001) used a Nd:YAG laser of 200 mJ pulsed for 10 nanosecond duration in air. Yan et al. used a 108 – 145 mJ Nd:YAG laser pulsed for a duration of 10 nanoseconds over a focal volume of 3 mm^3 to induce breakdown in air. The experimental data show a wide separation in time–scales between the laser pulse duration and observations of the blast wave and toroidal vortex. As seen above, the laser is pulsed on a time–scale of 10 nanoseconds. The blast wave, on the other hand is observed on a time–scale of 10 to 100 microseconds. This three to four order of magnitude separation in time–scale suggests that the plasma may be considered to be formed instantaneously to a first approximation, to evaluate its gasdynamic effect on the surrounding fluid.

*Graduate Research Assistant

†Assistant Professor

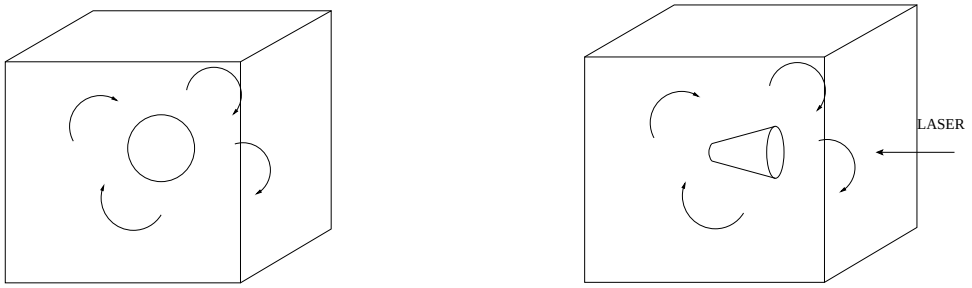

Figure 1. Schematic illustrating the thermal interaction between isotropic turbulence and spherical and conical idealizations of a region of plasma.

Various models have been investigated to better understand different features of this phenomenon. Similarity laws proposed by Taylor (1950), Sedov (1959) and Von Neumann (1963) for the radius and speed of the blast wave produced from a point source apply to the early stages of the blast wave, when it is strong. Note however that at early stages, the blast wave need not be spherical, which reduces applicability of the classical analysis. Brode (1955) performed a numerical simulation of the blast wave and concluded that the ideal gas assumption was reasonable for shock pressures less than 10 atmospheres in air. Steiner et al. (1998) perform computations using a real gas model to show that, when initialized with a self similar strong shock solution, the shock radius in the real gas model is quite close to that predicted by the classical point source explosion in an ideal gas. Other computations of blast wave propagation in quiescent air include those by Jiang et al (1998) and Yan et al. (2003). Dors et al. (2000) present a computational model which considers the asymmetry of laser energy deposition as well as ionization and dissociation effects on fluid properties. The initial stages of plasma formation due to laser energy deposition were modeled by Kandala and Candler (2002).

This paper considers the generation of a plasma region in a turbulent flow. The turbulence is assumed to be spatially homogeneous and isotropic prior to generation of the plasma. Only the thermal effects of the plasma are considered. As discussed above, this idealization is prompted by data that show that plasma generation occurs on the order of a nanosecond, while the blast wave is formed on the order of a microsecond, and interacts with the background flow on the order of hundreds of microseconds. Generating a plasma in a turbulent flow introduces the following physical parameters: size of the plasma region L as compared to the turbulence length scale λ, temperature excess of the plasma region T/T_0 (where T_0 denotes the background mean temperature), the fluctuation Mach number M_t and the turbulent Reynolds number Re_λ of the background turbulent flow. The effects of the variation of the first two parameters for a given M_t and Re_λ are discussed in this paper.

Two types of initial conditions have been used in the simulations (figure 1) – spherical and conical. The spherical initial condition corresponds to a point plasma region, while the conical initialization attempts to model the tear–drop shape of the plasma. For the spherical initialization, the temperature is kept constant within the radius of the sphere, and then decays as a Gaussian to the background temperature. For the conical initialization, a region in the shape of a conical frustum with radius R_1 and R_2 ($R_1 > R_2$)and length L is heated. Temperature varies exponentially along the axis of the cone such that T_1 and T_2 ($T_1 < T_2$) are temperatures at the center of the sections of the cone with radius R_1 and R_2 respectively. Also, the temperature decreases in the radial direction following a similar Gaussian pattern at any radial section.

A Fourier spectral solver was developed for the simulations. The solver assumes periodic boundary conditions, which are a valid approximation for homogeneous turbulence whose integral lengthscale is small compared to the domain size. However, the turbulence is no longer spatially homogeneous once the plasma is introduced. If the plasma is assumed spherical in nature, then the flow would statistically vary radially

and in time. If the plasma is assumed to be conical, the flow would be axisymmetrically homogeneous and nonstationary in time. For both cases, the periodic boundary conditions would require that the blast wave generated by the plasma only travel to distances small as compared to the domain size.

This paper is organized as follows. Section II describes details of the algorithm used (subsection A) and validation tests performed (subsection B). Laminar simulations in a quiescent background gas are discussed in section III. Spherical and conical idealizations are contrasted in subsections A and B respectively. A conical plasma region in background turbulence is considered in section C. A short summary in section IV concludes the paper.

II. Simulation methodology

A. Algorithm description

The governing equations are the continuity, and compressible Navier-Stokes equations for an ideal gas,

$$\frac{\partial \rho}{\partial t} + \frac{\partial \rho u_i}{\partial x_i} = 0, \tag{1a}$$

$$\frac{\partial \rho u_j}{\partial t} + \frac{\partial \rho u_j u_i}{\partial x_i} = -\frac{\partial}{\partial x_i}\left[p\delta_{ij} - \frac{\mu}{Re}\left(\frac{\partial u_i}{\partial x_j} + \frac{\partial u_j}{\partial x_i} - \frac{2}{3}\frac{\partial u_k}{\partial x_k}\delta_{ij}\right)\right], \tag{1b}$$

$$\frac{\partial \rho e_T}{\partial t} + \frac{\partial \rho e_T u_i}{\partial x_i} = \frac{\partial}{\partial x_i}\left[-pu_i + \frac{\mu}{Re}\left(\frac{\partial u_i}{\partial x_j}\frac{\partial u_j}{\partial x_i} - \frac{2}{3}\frac{\partial u_k}{\partial x_k}\delta_{ij}\right)u_j\right] + \frac{\partial}{\partial x_i}\left(\frac{\mu}{(\gamma-1)RePr}\frac{\partial T}{\partial x_i}\right) \tag{1c}$$

where all the variables are non–dimensionalized with respect to their initial mean values. The equation of state is

$$p = \rho T/\gamma, \tag{2}$$

where the temperature is related to the internal energy as

$$T = \gamma(\gamma-1)e, \tag{3}$$

and the total energy is related to internal energy and kinetic energy as

$$\rho e_T = \rho e + \frac{1}{2}\rho u_i u_i. \tag{4}$$

The Reynolds number and Prandtl number are given by

$$Re = {\rho_0}^* {c_0}^* {L_0}^* / {\mu_0}^*; \quad Pr = {\mu}^* {c_p}^* / {k}^*. \tag{5}$$

Here, the subscript '0' denotes initial mean values and the superscript, '*' denotes dimensional variables. c_0^* is the speed of sound based on initial mean temperature; i.e.

$${c_0}^* = (\gamma R^* {T_0}^*)^{1/2}. \tag{6}$$

μ^* and k^* are dimensional coefficients of viscosity and thermal conductivity, and ${c_p}^*$ is the specific heat at constant pressure. The Prandtl number is assumed to be constant and equal to 0.7, and the gas is assumed to be diatomic i.e. $\gamma = 1.4$. Viscosity is assumed to follow the power law dependence,

$$\mu = T^{0.67}. \tag{7}$$

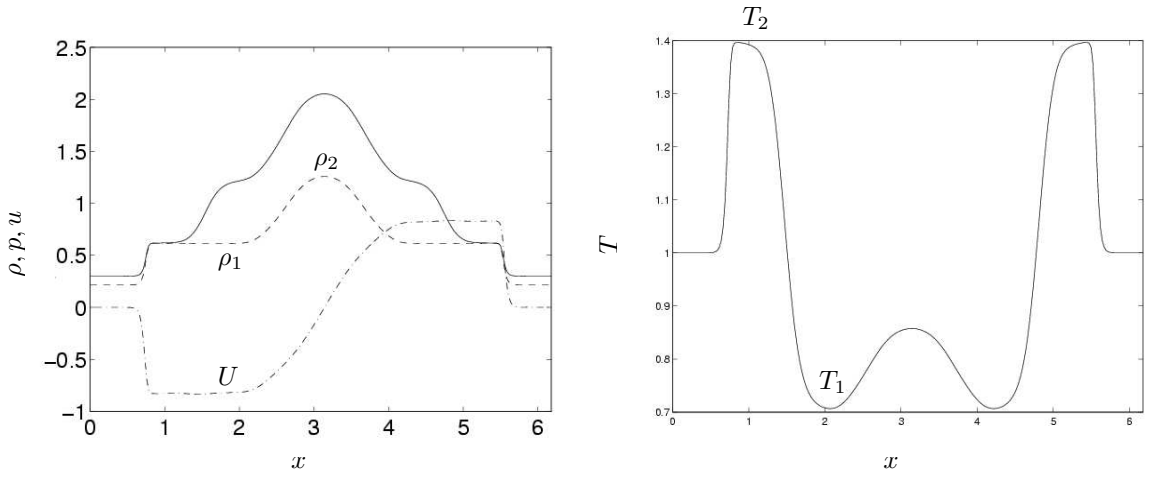

Figure 2. Results for periodic shock tube problem at $t = 1$. The first figure shows density (———), pressure (– – – –) and velocity (—·—). Temperature is shown in the second figure.

The Navier-Stokes equations are solved using Fourier methods to compute the spatial derivatives. Any variable f is discretely represented as

$$f(x_1, x_2, x_3) = \sum_{k_1=-N_1/2}^{N_1/2-1} \sum_{k_2=-N_2/2}^{N_2/2-1} \sum_{k_3=-N_3/2}^{N_3/2-1} \hat{f}(k_1, k_2, k_3) \mathrm{e}^{(k_1 x_1 + k_2 x_2 + k_3 x_3)} \tag{8}$$

where $\hat{f}(k_1, k_2, k_3)$ are the Fourier coefficients of f, and N_1, N_2 and N_3 are the number of points used to discretize the domain along x_1, x_2 and x_3 respectively. The Fourier coefficients of the spatial derivatives are therefore

$$\widehat{\frac{\partial f}{\partial x_i}} = ik_i \widehat{f}, \quad \widehat{\frac{\partial^2 f}{\partial x_\alpha x_\alpha}} = -k_\alpha^2 \widehat{f}. \tag{9}$$

A colocated approach is used, and the solution is advanced in time using a fourth order Runge-Kutta scheme. The skew–symmetric form of the convection terms

$$\frac{\partial fg}{\partial x_j} = \frac{1}{2}\left(\frac{\partial fg}{\partial x_j} + f\frac{\partial g}{\partial x_j} + g\frac{\partial f}{\partial x_j}\right), \tag{10}$$

is used to suppress aliasing errors resulting from the nonlinear convection terms (Blaisdell 1991). The above algorithm is implemented for parallel platforms using MPI. The library FFTW is used to compute Fourier transforms, and a pencil data structure is used. Each processor stores data along the entire extent of the x_1- direction, while data along the x_2- and x_3- directions are equally distributed among the processors. Fourier transforms along the x_1- direction are therefore readily computed, while transforms in the other directions require that the data be transposed prior to transforming.

B. Validation results

1. Shock tube problem

This is a one-dimensional periodic problem where fluid is initially at rest at constant temperature, and the initial pressure is higher at the center of the domain compared to its value at the boundaries. The initial pressure gradient sets up a shock wave and expansion wave that propagate through the domain. The length

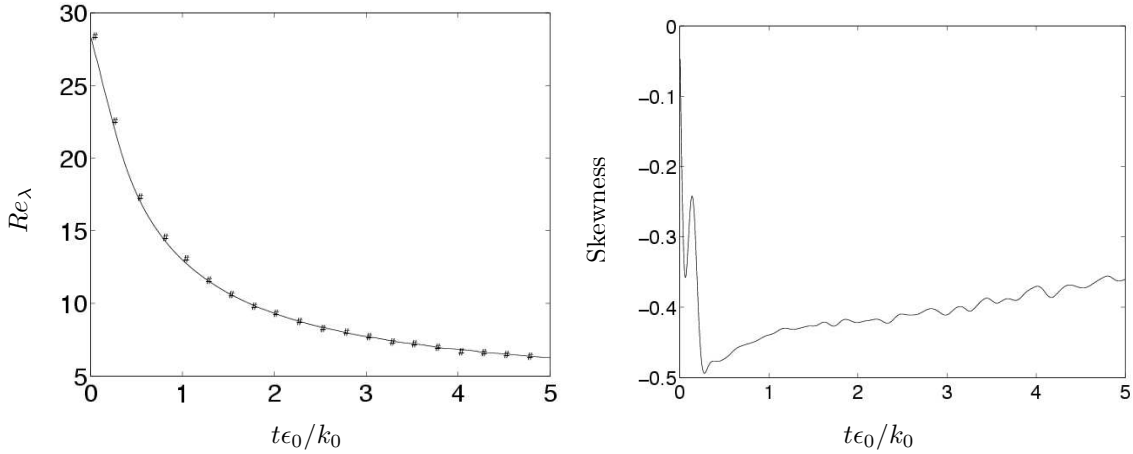

Figure 3. DNS of isotropic turbulence compared to simulations by Blaisdell et al. (1991). The two figures show the time evolution of Re_λ and velocity–derivative skewness respectively. Solid lines are simulation results and symbols are data from Blaisdell et al. (1991). Time is non–dimensionalized using the initial dissipation ϵ_0 and kinetic energy (k_0).

of the domain is 2π and the initial density profile is set to vary between 0.3 and 3.0. The initial temperature $T = 1$ and pressure is obtained using the equation of state. The computation is performed on a 256-point grid with a time step of 0.001 and dynamic viscosity = 0.005. Figure 2 shows instantaneous profiles of the solution. Comparison of density, pressure, velocity and temperature jumps at a later time ($t = 1.0$) to analytical solution in table 1 shows that all results obtained are within 1% error. Here u is the magnitude of maximum velocity along x, ρ_1 is the peak value of density at the shock front, ρ_2 is the peak value of density across the contact discontinuity, and T_1 and T_2 are the minimum and maximum temperature attained (figure 2).

Table 1. Comparison between predicted and calculated values for shock tube

	ρ_1	ρ_2	T_2	T_1	U
Predicted	0.613	1.223	1.393	0.698	0.821
Calculated	0.612	1.224	1.401	0.695	0.827

2. Isotropic turbulence

Direct numerical simulation of isotropic turbulence was performed under conditions corresponding to past DNS by Blaisdell et al. (1991). The initial velocity fluctuations are isotropic and divergence–free, while initial fluctuations in pressure, temperature and density are assumed to be zero. The initial velocity fluctuations are generated using Rogallo's (1981) method. The Fourier coefficients of the initial velocity fields are given by

$$\hat{u} = \frac{\alpha k k_2 + \beta k_1 k_3}{k({k_1}^2 + {k_2}^2)^{1/2}} e_1 + \frac{\beta k_2 k_3 - \alpha k k_1}{k({k_1}^2 + {k_2}^2)^{1/2}} e_2 - \frac{\beta({k_1}^2 + {k_2}^2)^{1/2}}{k} e_3 \tag{11}$$

where

$$\alpha(k) = \frac{E(k)}{4\pi k^2}^{1/2} \mathrm{e}^{i\theta_1}\cos(\phi), \quad \beta(k) = \frac{E(k)}{4\pi k^2}^{1/2} \mathrm{e}^{i\theta_2}\cos(\phi). \tag{12}$$

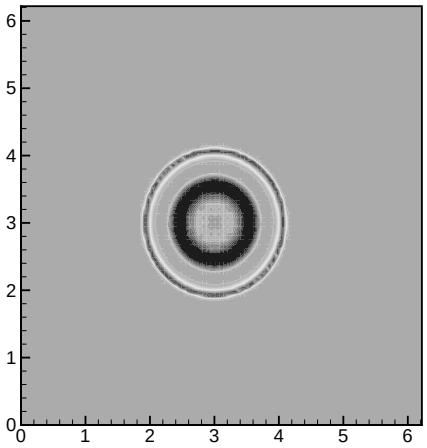

Figure 4. Instantaneous solution in $x-y$ plane for spherical idealization of plasma in laminar quiescent background gas. Contour plot of pressure at $t = 1.0$ showing propagation of blast wave in flow at rest.

Here θ_1, θ_2 and ϕ are random numbers from 0 to 2π, and e_i denote the unit vectors along the three coordinate directions.

The initial energy spectrum is a top hat spectrum as used by Blaisdell et al. (1991, case idc96). This spectrum has energy only in scales represented by wave numbers $k = 8$ through 16. The initial fluctuation Mach number $M_t = 0.3$, and Taylor microscale Reynolds number $Re_\lambda = 50$. Figure 3 compares the time evolution of Re_λ to Blaisdell et al's results, and good agreement is observed. Also shown is the time evolution of the mean velocity–derivative skewness, $S_\alpha = \overline{(\frac{\partial u_\alpha}{\partial x_\alpha})^3}/\overline{(\frac{\partial u_\alpha}{\partial x_\alpha})^2}^{3/2}$ which relaxes to a nearly constant value once the turbulence has relaxed from its initial conditions.

III. Laminar simulations

Here, the background flow is initially at rest, and energy is then added locally to the flow. This is achieved by increasing the temperature and pressure in the plasma region while keeping the density constant. This region of elevated temperature may either be spherical or conical as shown in figure 1. The objective of the laminar simulations is to ensure that the computations reproduce features seen in experiment, and to contrast the spherical and conical idealizations. Also, the laminar solutions will qualitatively approximate the mean flow observed when the plasma is generated in isotropic turbulence.

A. Spherical initialization

Here a spherical region of the flow is heated at the center of the domain. The simulations are performed for an initial temperature ratio $T/T_0 = 3$. Energy is added in two different length scales: $R = 0.2$ and $R = 0.1$ in a domain of 2π.

Figure 4 shows contour plots of pressure at $t = 1.0$. A spherical shock front is clearly seen. Radial profiles of density, pressure and temperature are shown in figure 5. The radial profiles show the shock front propagating radially outward leaving behind a radially expanding flow. The intensity of the shock front is seen to decrease in time as expected from its increasing radius. Recall that both features are observed in experiment. Note that if this plasma were generated in a turbulent flow, then the expansion at the center would suppress turbulent fluctuations and increase their lengthscale, while the shock wave would increase turbulence levels and decrease turbulence lengthscales (e.g. Mahesh et al. 1995, 1997). The decrease in shock

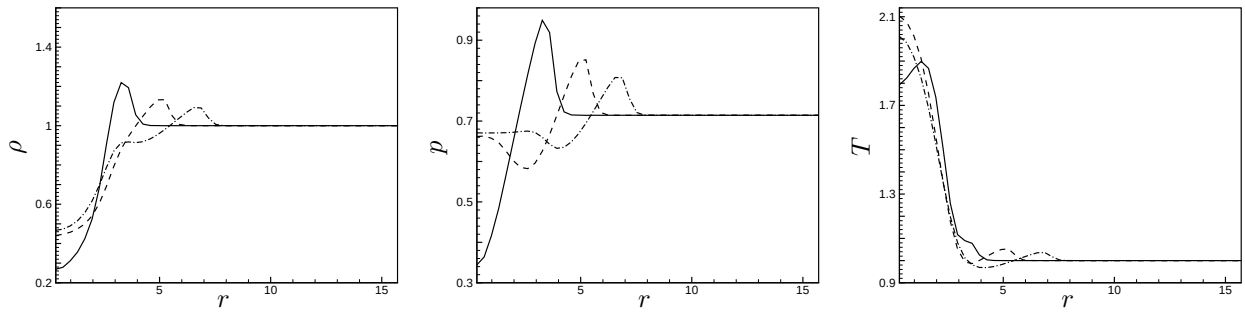

Figure 5. Time evolution of solution for spherical idealization of plasma in laminar quiescent background gas. Radial mean profiles of density, pressure and temperature in time, ——— : $t = 0.3$, - - - - : $t = 0.6$ and —·— : $t = 0.9$.

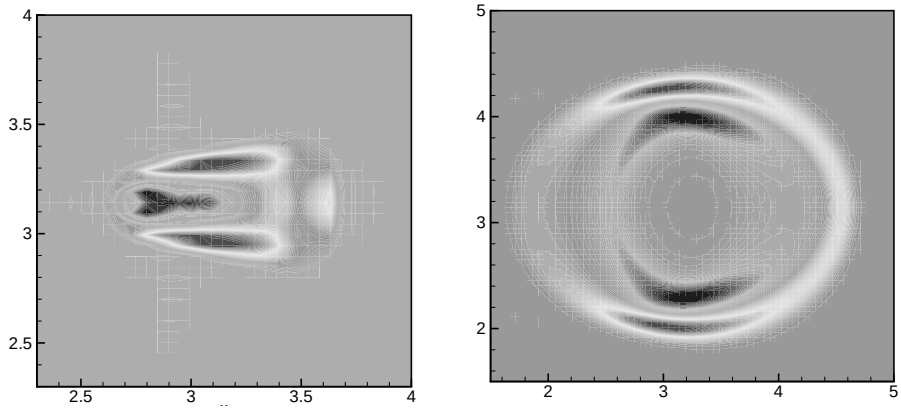

Figure 6. Instantaneous solution for conical idealization of plasma in quiescent background gas. Contour plots of pressure at $t = 0.3$ and $t = 1.0$ shows initial tear drop shaped blast wave that eventually becomes spherical in nature.

strength with increasing radial distance means that the extent to which turbulence is compressed decreases with increasing radius. This would cause a strong radial gradient in turbulence properties which would mean than inhomogeneous turbulence transport would be quite important. This behavior is quite different from that when homogeneous turbulence interacts with a plane shock wave (e.g. Mahesh et al. 1995, 1997).

The spherical initialization predicts experimentally observed behavior of the blast wave. However, the toroidal ring vortex that is experimentally observed is not observed in the simulations. While relatively unimportant in a background quiescent flow, the ring–vortex is likely to be quite important to background turbulence since its length scale is comparable to that of the initial plasma region, which depending upon the Reynolds number could be comparable to the turbulence lengthscale. The toroidal vortex would therefore be expected to interact with the background turbulence.

B. Conical Initialization

In this case a conical frustum is heated at the center of the domain. The conical frustum is chosen as an approximation to the tear–drop shape of the plasma region that is experimentally observed. Even though the laser is focused on a spherical region, the heated ions tend to move axially toward the source of heating, thus attaining the shape of a conical frustum. To study the effect of addition of energy in different length-scales, simulations have been performed with the length of the frustum L being $\pi/2$ and $\pi/6$ on a domain of 2π.

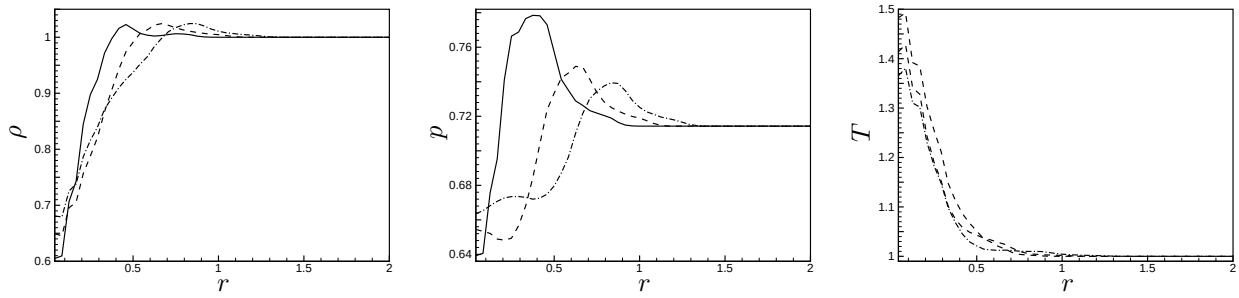

Figure 7. Time evolution of solution for conical idealization of plasma in quiescent background gas. Radial mean profiles of density, pressure and temperature in time, ——— : $t = 0.3$, - - - - : $t = 0.6$ and —·— : $t = 0.9$.

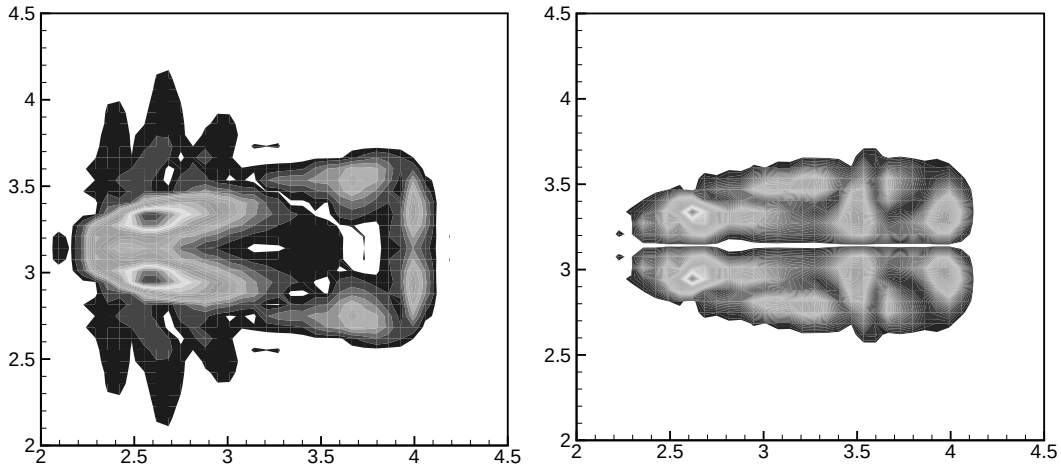

Figure 8. Illustration of the generation of toroidal vortex by baroclininc means for conical idealization of plasma in laminar quiescent background gas. The first figure shows contours of vorticity magnitude in $x - y$ plane for $L = \pi/2$ at $t = 0.3$. The second figure shows contours of baroclinic vorticity at the same instant.

The temperature ratios used in the simulations are $T_1/T_0 = 3,\ T_2/T_0 = 1.5$ and $T_1/T_0 = 5,\ T_2/T_0 = 2.5$.

As a result of heat being added locally a blast-wave is formed. This blast-wave initially has a tear-drop shape but becomes spherical as it propagates to a radius which is about 3 to 4 times the length of the frustum. This is evident from the contour plots of pressure in time (figure 6). The plots at $t = 0.1$ and $t = 1.0$ show steady development into a spherical shape from the initial tear-drop shape. Unlike the spherical idealization, the conical idealization is not spherically symmetric; instead it is axisymmetric along the axis of the conical frustum. In this case, plotting radial mean profiles would be inaccurate as long as the blast wave is tear-drop shaped. However if one starts with a very small length L then the wave becomes spherical at a small radius and so plotting radial mean profiles will still be a good approximation. This is evident from the plots of radial mean profiles of density, pressure and temperature (figure 7). The profiles show similar behavior as in the spherical initialization case; i.e. a blast wave propagates out leaving behind an expanding region of elevated temperature. In the initial stages, note that most of the pressure rise occurs normal to the axis of the cone.

Another important feature of the conical idealization is that vorticity is generated at the outer edges of the plasma. Figure 8 shows contours of vorticity at time $t = 0.3$. Note that the vorticity is most intense near the smaller end of the cone, and in three–dimensions is toroidal in nature. A more quantitative evolution

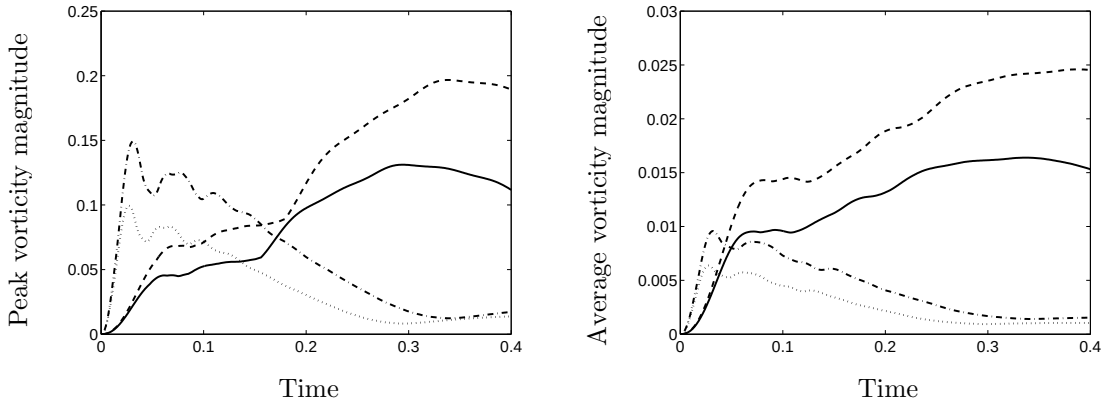

Figure 9. Time evolution of vorticity for conical idealization of plasma in laminar quiescent background gas. Plots of peak vorticity and average vorticity in time are shown. ····· : $L = \pi/2$ and temperature ratios 3 to 1.5, ——— : $L = \pi/6$ and temperature ratios 3 to 1.5, —·— : $L = \pi/2$ and temperature ratios 5 to 2.5, - - - - : $L = \pi/6$ and temperature ratios 5 to 2.5.

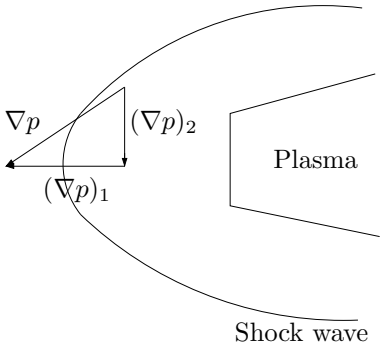

Figure 10. Schematic illustrating the effect of the tear–drop shaped blast wave on the alignment between density and pressure gradients.

is shown in figure 9 where the peak value of vorticity, and the average vorticity in the domain are plotted against time. Note that the vorticity increases rapidly in the initial stages; it then decreases for the $L = \pi/2$ plasma while it continues increasing for the $L = \pi/4$ plasma. Also, the peak vorticity is higher for the higher temperature plasmas. This behavior is explained by the evolution equation for vorticity:

$$\frac{D\vec{\omega}}{Dt} = \underbrace{(\vec{\omega}\cdot\nabla)\vec{u}}_{\text{vortex stretching/tilting}} - \underbrace{\vec{\omega}(\nabla\cdot\vec{u})}_{\text{bulk compression}} - \underbrace{\frac{\nabla p\times\nabla\rho}{\rho^2}}_{\text{baroclinic}}. \tag{13}$$

The viscous term is omitted in the above equation. Figure 8 shows contour plots of the baroclinic term for the case with $L = \pi/2$. Note that the baroclinic term is most intense in the regions where the vorticity was seen to be highest; i.e. near the smaller end of the conical region. Comparison of the magnitude of the baroclinic term to other terms in the vorticity equations show that the baroclinic term is significantly larger in magnitude during the initial stages, and is therefore responsible for generation of the toroidal vorticity.

This also explains why the vorticity is most intense around the edges of the smaller face of the cone.

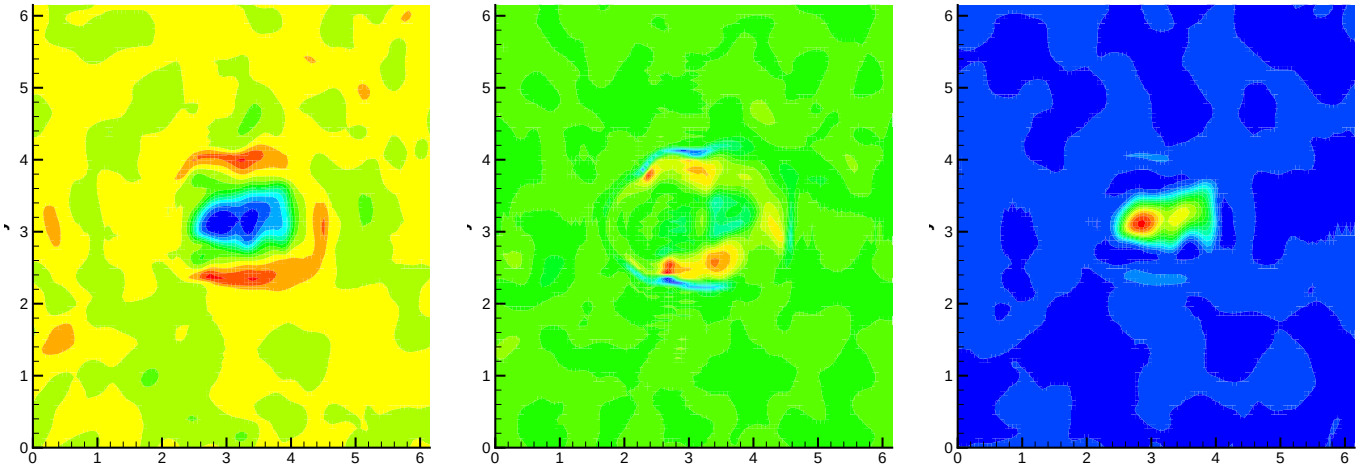

Figure 11. Instantaneous contours of density, velocity divergence and temperature in interaction of conical idealization of plasma region with background turbulence at $t = 1$.

Recall that the blast wave is initially conical or tear–drop shaped. The radius of curvature of the blast wave therefore varies along its length. Figure 10 shows a schematic of this process. It is well known that curved shock waves results in misalignment between the density and pressure gradients and produce baroclinic vorticity as a result. Consider figure 10. The tear–drop shaped shock wave is curved near the leading and trailing edges. Gradients in density and pressure $(\nabla p)_1$ and $(\nabla \rho)_1$ are developed along the axial direction due to the interaction of shock wave with the flow upstream. However, due to the curved nature of the shock wave the magnitude of these gradients varies with angular distance from the axis of the cone; they decrease as the shock becomes more inclined. As a result, there is an angular variation in fluid properties down–stream of the shock resulting in secondary gradients $(\nabla p)_2$ and $(\nabla \rho)_2$. The net gradient is the vector sum of these two gradients as shown. Since the density and pressure jumps are different across the curved shock by the Rankine–Hugoniot conditions, the direction of the resultant gradient vector is different for density and pressure. Thus, there is a misalignment between the density and pressure gradients behind the shock. This results in generation of baroclinic vorticity.

The gradients would be expected to increase as the radius of curvature of the shock wave decreases. Maximum baroclinic vorticity is therefore generated near the smaller side of the cone because near the smaller side, the radius of curvature of the shock is the smallest. Recall (figure 9) that higher levels of vorticity were obtained for the smaller conical region. This is because, for the same temperature ratio, a more compact plasma generates higher gradients, and therefore higher levels of the baroclinic term.

C. Turbulent Simulations

In the case of the turbulent simulations, the background flow is developed isotropic turbulence. The turbulence is initialized as described in section IIB with initial fluctuation Mach number $M_t = 0.3$ and turbulent Reynolds number $Re_\lambda = 50$. This turbulent field is allowed to decay for some time after which the velocity derivative skewness attains a steady value in the range of -0.3 to -0.4. Energy is then added locally to the flow and its behavior is observed. Only the conical idealization is considered. The length of the conical frustum $L = 0.5\lambda$ and temperature ratios of $T_1/T_0 = 3$ and $T_2/T_0 = 1.5$ on a domain of length 2π.

Figure 11 shows instantaneous contours of density, temperature and divergence of velocity. Note that the regions of compression and expansion are most intense normal to the axis of the plasma region. The

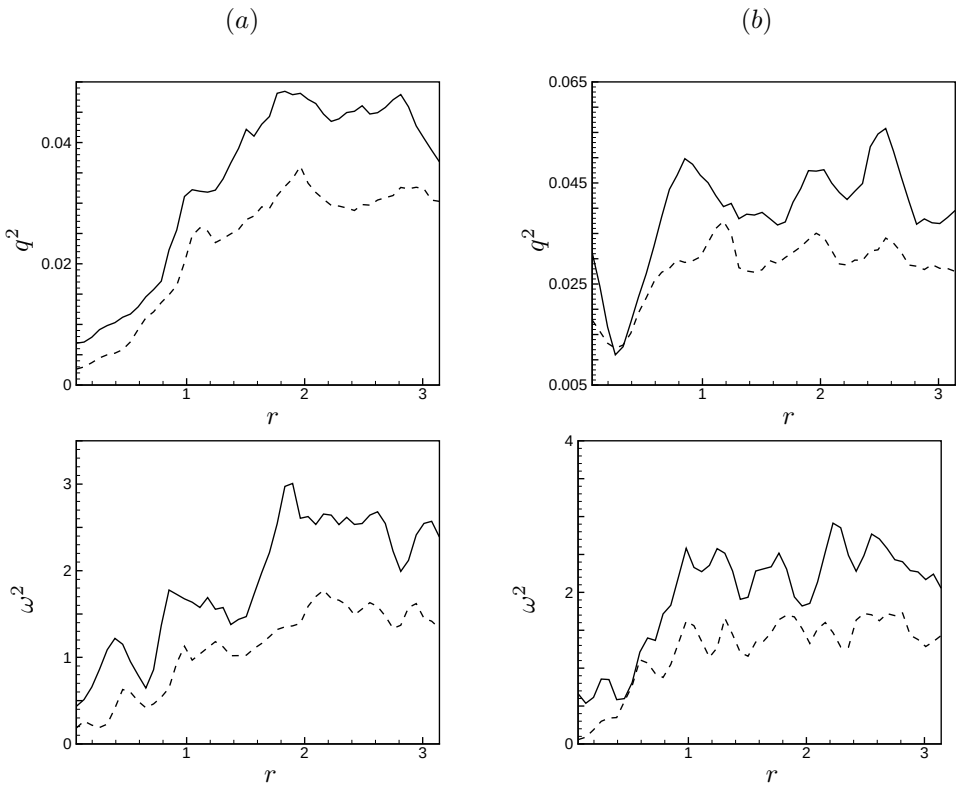

Figure 12. Radial profiles of twice the turbulence kinetic energy (q^2) and vorticity fluctuation magnitude squared (ω^2) in interaction of conical idealization of plasma region with background turbulence. (a)**: t=1,** (b)**: t=2.** ——— **: trailing edge of plasma,** – – – – **: center of plasma.**

divergence of velocity shows a leading region of compression followed by expansion. The flow also expands near the larger edge of the plasma (leading edge with respect to the laser). The distortion of the plasma region and the blast wave by the turbulence is clearly apparent.

This behavior affects turbulence levels as shown in figure 12. Note that the turbulence is statistically homogeneous in axisymmetric planes with respect to the axis of the conical region. Statistics were therefore computed in $x - r$ planes. Radial profiles of turbulence kinetic energy and vorticity are shown at two stations along the axis of the plasma in figure 12. The turbulence is seen to be suppressed in the region occupied by the plasma and slightly amplifies across the blast wave. The suppression in the plasma region is consistent with both expansion of the mean flow near the center and increasing viscosity due to the increased temperature. The compression in the blast wave is expected to increase turbulence levels (e.g. Mahesh et al. 1995, 1997); however this amplification depends on the strength of the blast wave. The temperature ratio in the present simulations is not high enough to set up a strong enough blast wave for this effect to be noticeable. It is expected that at higher temperature ratios, the turbulence in the plasma region will be suppressed, turbulence levels will increase across the blast wave, and turbulence away from the plasma region will decay due to viscosity. Future simulations at higher temperature ratio and computation of the kinetic energy budget will examine this behavior.

IV. Summary

This paper uses direct numerical simulation to study the thermal effect of a region of plasma on isotropic turbulence. The simulations solve the compressible ideal gas Navier–Stokes equations using Fourier spectral methods. Two idealizations of the plasma – spherical and conical are contrasted using laminar simulations

of the plasma in quiescent air. The conical idealization is found preferable in that it produces a toroidal region of vorticity as observed experimentally. The vorticity evolution equation shows that baroclinic effects are responsible for production of the vorticity. This observation explains qualitatively observed trends of the vorticity with plasma size and temperature ratio. Derivation of a quantitative scaling law is in progress. Preliminary simulations of a conical plasma in background turbulence were performed. The mean field associated with the plasma consists of a blast wave followed by a region of expansion propagating normal to the axis of the plasma. The leading edge of the plasma also shows significant mean expansion. Turbulence levels are suppressed in the region of the plasma, presumably due to mean expansion. Future work will evaluate if these trends persist at higher temperature ratios and more compact plasma regions.

Acknowledgments This work is supported by the United States Air Force Office of Scientific Research under grant FA-9550-04-1-0064. Computing resources were provided by the Minnesota Supercomputing Institute, the San Diego Supercomputing Center, and the National Center for Supercomputing Applications. We are grateful to Mr. Yucheng Hou for useful discussions during the course of this project.

References

[1]D. Knight, V. Kuchinskiy, A. Kuranov & E. Sheikin, 2003, Survey of aerodynamic flow control at high speed by energy deposition, *AIAA paper 2003–0525*.

[2]R.G. Adelgren, H. Yan, G.S. Elliot, D. Knight, T.J. Beutner, A. Zheltovodov, M. Ivanov & D. Khotyanovsky, 2003, Localized flow control by laser energy deposition applied to Edney IV shock impingement and intersecting shocks, *AIAA paper 2003–31*.

[3]M.N. Scheider, S.O. Macheret, S.H. Zaidi, I.G. Girgis, Yu. P. Raizer & R.B. Miles, 2003, Steady and unsteady supersonic flow control with energy addition, *AIAA paper 2003–3862*.

[4]P. Maker, R. Terhune & C. Savage, 1963, *Proccedings of the Third International Quantum Mechanics Conference*, Paris.

[5]E. Damon & R. Tomlinson, 1963, Observation of ionization of gases by a ruby laser, *Applied Optics*, **2(5)**.

[6]R. Meyerand & A. Haught, 1963, Gas breakdown at optical frequencies, *Phys. Rev. Let.*, **11(9):** 401–403.

[7]Yu. P. Raizer, 1997, *Gas discharge physics*, 2nd edition, Springer–Verlag, New York.

[8]Z. Jiang, K. Takayama, K.P.B. Moosad, O. Onodera & M. Sun, 1998, Numerical and experimental study of a micro-blast wave generated by pulsed laser beam focusing, *Shock waves*, **8:** 337–349.

[9]J. Lewis, C. Parigger, J. Hornkohl &G. Guan, 1999, Laser–induced optical breakdown plasma spectra and analyses by use of the program NEQAIR, *AIAA paper 99–0723*.

[10]I. Dors, C. Parigger & J. Lewis, 2000, Fluid dynamic effects following laser–induced optical breakdown, *AIAA paper 2000–0717*.

[11]R. Adelgren, M. Boguszko & G. Elliott, 2001, Experimental summary report–shock propagation measurements for Nd:YAG laser induced breakdown in quiescent air, Department of Mechanical and Aerospace Engineering, Rutgers University.

[12]H. Yan, M. Adelgren, M. Bouszko, G. Elliott & D. Knight, 2003, Laser energy deposition in quiescent air, *AIAA paper 2003–1051*.

[13]G.I. Taylor, 1950, The formation of a blast wave by a very intense explosion: I theoretical discussion, *Proc. Roy. Soc.*, **201:** 159–174.

[14]L.I. Sedov, 1958, *Similarity and dimensional methods in mechanics*, Academic, New York.

[15]J. Von Neumann, 1963, The point source solution, *Collected works of J von Neumann, Vol. VI*, Pergamon, England.

[16]H.L. Brode, 1955, Numerical solution of blast waves, *J. Appl. Phys.*, **26(6):** 766–775.

[17]H. Steiner, W. Gretler & T. Hirschler, Numerical solution for spherical laser–driven shock waves, *Shock waves*, **8:** 337–349.

[18]R. Kandala & G. Candler, 2002, Computational modeling of localized laser energy deposition in quiescent air, *AIAA paper 2002–2160*.

[19]R.S. Rogallo, 1981, Numerical experiments in homogeneous turbulence, *NASA Tech. Memo.* 81315.

[20]G.A Blaisdell, N.N. Mansour and W.C Reynolds, 1991, Numerical simulations of compressible homogeneous turbulence, Report No TF-50, Thermosciences Division, Department of Mechanical Engineering, Stanford University.

[21]K. Mahesh, S.K. Lele & P. Moin, 1995, The interaction of an isotropic field of acoustic waves with a shock wave, *J. Fluid Mech.*, **300:** 383–407.

[22]K. Mahesh, S.K. Lele & P. Moin, 1997, The influence of entropy fluctuations on the interaction of turbulence with a shock wave, *J. Fluid Mech.*, **334:** 353–379.